Time-Resolved Compression of a Spherical Shell with a Re-Entrant Cone to High Areal Density for Fast-Ignition Laser Fusion

The compression of matter to a very high density is of general interest for high-energy-density physics,[1] laboratory astrophysics,[2] and inertial confinement fusion (ICF).[3] This article reports on picosecond, time-resolved, monochromatic 8-keV x-ray radiographic measurements of imploded cone-in-shell targets on the OMEGA laser. The results show that a spherical shell with a re-entrant cone—a system with broken spherical symmetry—can be successfully compressed with long-pulse (~ns) lasers to a final mass density and geometry that provide favorable characteristics for subsequent ignition with a short-pulse (~ps) laser. We find excellent agreement with predictions from two-dimensional (2-D) radiation–hydrodynamic simulations with the code *DRACO*.[4] This work is an important step forward for fast ignition[5] because it demonstrates that sufficient areal density can be assembled at the tip of the re-entrant cone to trap the fraction of the fast-electron energy spectrum (~MeV) from the short-pulse laser that is relevant for fast ignition.

Over the last four decades, a tremendous effort has been devoted to studying the physics of high-density matter by compressing spherical shells with powerful laser beams.[6,7] Achieving high compression with pressures $\sim 10^{16}$ Pa is vital for ICF, where a few milligrams of frozen deuterium and tritium fuel are compressed by laser light ablation (direct drive) or by x-ray ablation (indirect drive) to such high temperatures and densities that ignition is reached and a thermonuclear burn wave spreads through the shell. Similar pressures found inside astrophysical objects make laboratory compression experiments interesting for studying those material states. Pressures of $\sim 10^{16}$ Pa prevail in the sun's core, while they are ~100× lower in the core of giant planets. An important step toward ignition has been recently demonstrated by measuring fusion energy that exceeds the energy coupled in the fuel in an ICF implosion.[8] So far, ignition has not been reached despite code predictions. Besides the conventional "hot-spot" approach, which triggers ignition in the center of a rapidly converging shell, alternative approaches such as fast ignition (FI)[5] and shock ignition (SI),[9] which separate the compression and ignition phases of the implosion, have been proposed. Ignition is achieved from highly localized heating: on the side of the high-density fuel using a separate ultrahigh-intensity laser (FI) or in the center of the compressed shell by a converging shock wave (SI). These concepts are attractive because higher gains might be achievable than with central hot-spot ignition. Early experiments studying the FI concept[10,11] reported a coupling efficiency of 15% to 30% of the short-pulse laser energy into the compressed plasma. Those experiments were limited by several factors, including insufficient drive-laser energy (2.5 kJ), no pulse-shaping capability, and a longer drive-laser wavelength (532 nm instead of 351 nm)—unfavorable factors for achieving high compression. In addition, the low number of overlapping drive beams resulted in a large illumination nonuniformity that affected the symmetry and possibly the hydrodynamic stability of the implosion. Laser pulse shaping is necessary to compress the target on a low adiabat (α), which is defined as the ratio of the plasma pressure in the shell to the Fermi pressure of a degenerate electron gas.[12] A low adiabat is a prerequisite for high target compression. Based on our experiments and simulations, we conclude that the FI experiments[10,11] were merely qualitative and were not guided by sufficient simulation capability to adequately describe this complicated radiation–hydrodynamic problem. It is therefore questionable whether sufficient compression was achieved to stop MeV electrons and surprising that such high coupling efficiencies were reported[10,11] (efficiencies that could not be reproduced in experiments on OMEGA[13]). Follow-up experiments at the Institute for Laser Engineering confirm an insufficient compression, being ~10× lower than was previously estimated, and a much lower (~1.6%) short-pulse beam-energy coupling.[14]

In the experiments reported here, thin plastic shells with an embedded hollow cone made out of high-Z material were imploded. The purpose of the cone was to provide a plasma-free path for the short-pulse ignition laser to propagate as close as possible to the dense fuel. One complication is that the cone breaks the spherical symmetry and requires multidimensional simulation capability to accurately model both the flow of the material and the interaction between radiation and matter. The picosecond, time-resolved radiographic measurements of the hydrodynamic evolution of cone-in-shell implosions presented

here demonstrate for the first time the assembly of plasma dense enough to stop MeV electrons at a time when the cone tip has not been breached by the implosion, which is an important requirement for fast ignition. This is possible only because of the unique experimental capability of the Omega Laser Facility and a significant improvement in multidimensional simulations. The excellent agreement between experiment and simulation obtained here provides a benchmark for the code calculations that will be used to further improve implosion performance.

Important quantities that characterize the fuel assembly are the mass-density distribution $\rho(r)$ and the areal density ρR, which is given by the integral of ρ over the spatial coordinate from the shell's center to infinity, $\int_0^\infty \rho dr$. Measurements of ρR and ρ provide a method to compare the actual and predicted implosion performances. Radiography with x rays in combination with a framing camera is a technique[15] to spatially measure and temporally resolve the fuel mass; it has been used on OMEGA to study the implosion dynamics of deuterium gas-filled plastic spherical shells without a cone using an ~5-keV broadband backlighter driven by an ~1-ns laser, and a camera with an ~40-ps integration time.[16] A mass-density distribution $\rho(r)$ and a ρR of up to ~60 mg/cm^2 were measured at various

times outside of peak compression.[16] In those experiments a strong x-ray self-emission from the hot core prevented a measurement at peak compression. Previous experiments with cone-in-shell targets in indirect[17] and direct drive[18,19] investigated high-adiabat implosions with simple square pulses, which lacked quantitative comparison to simulations.

The current experiment used thick (42-μm) plastic shells with a cone and a low gas pressure (~0.8 atm of air) imploded by a shaped laser pulse to minimize x-ray self-emission. An x-ray source driven by a short pulse with a shorter emission time and a higher photon energy combined with a narrow-bandwidth ($\Delta E/E = 1.2 \times 10^{-3}$) crystal imager provided the necessary tool to study the fuel assembly in unprecedented detail. The mass-absorption coefficient μ of the compressed material is a function of the photon energy, and measuring it with a spectrally pure photon source significantly decreases the uncertainty in the inference of mass density and areal density. Figure 139.34(a) shows the experimental setup. The cone-in-shell target [Fig. 139.34(b)] consisted of a hollow gold cone mounted inside a plastic shell. A small aluminum cylindrical tip was mounted on the end of the cone. The purpose of the 60-μm-thick Al tip was to delay the shock breakout
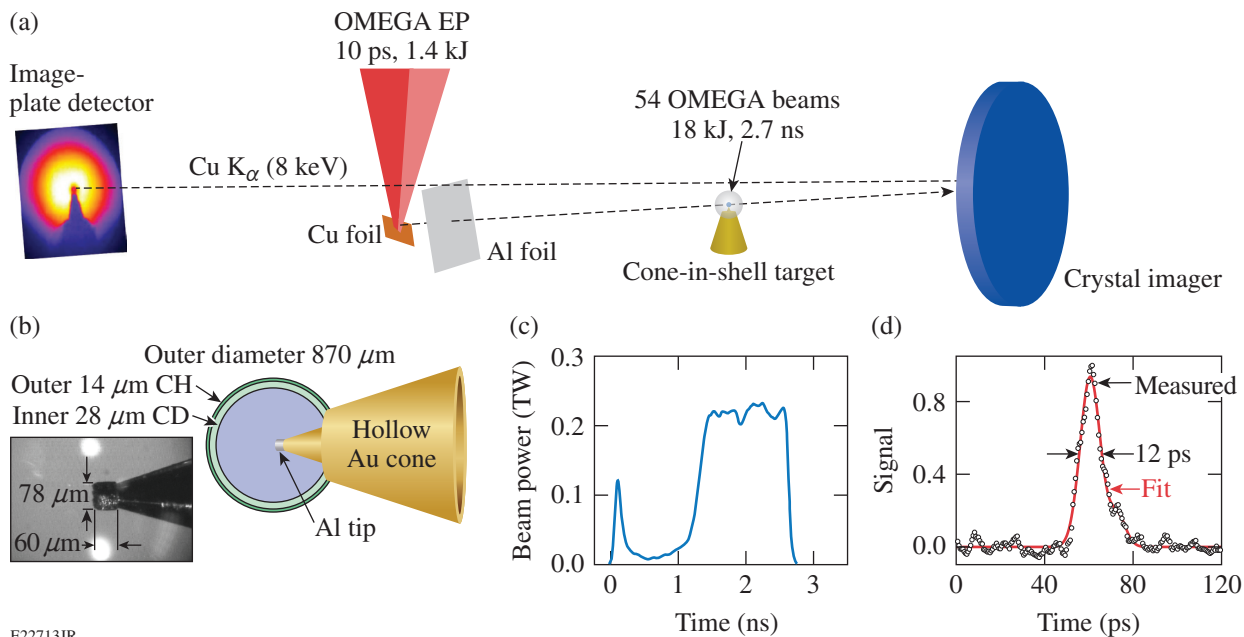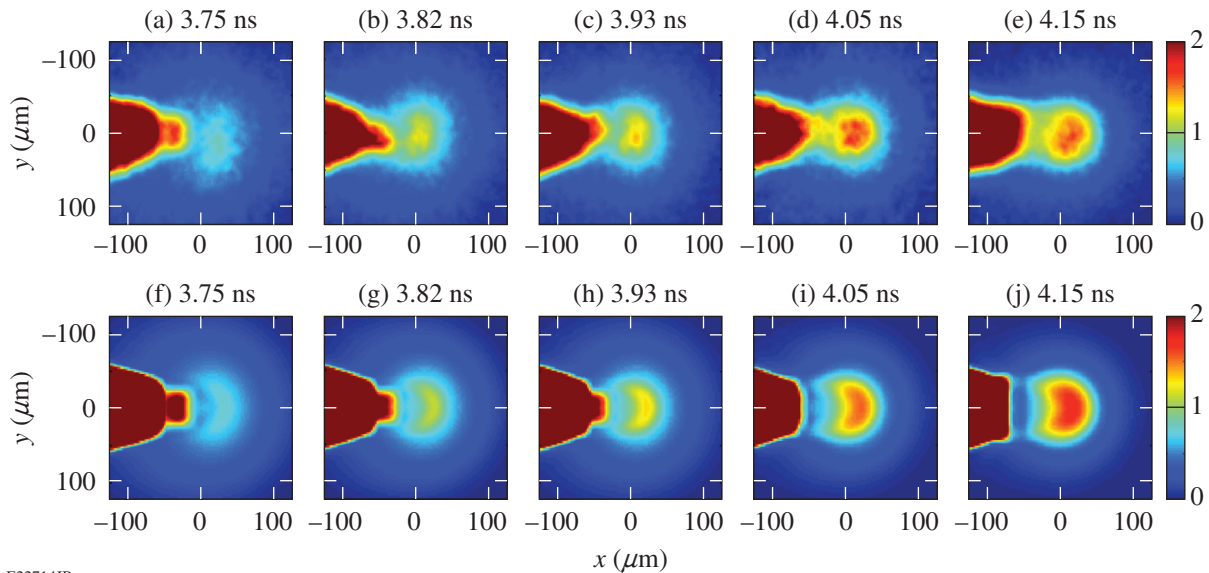

Figure 139.34
(a) Schematic of the setup of the backlighter experiment with a Cu foil irradiated by the OMEGA EP short-pulse beam and using 54 OMEGA beams to implode a cone-in-shell target. A 50-μm-thick Al foil was located 2 mm from the Cu foil to shield it from plasma and x-ray radiation from the implosion. A raw image of the fuel assembly is shown in the image plane. The distances are not to scale. (b) Illustration of the cone-in-shell target. (c) Laser pulse shape to implode the capsule. (d) Time-resolved K$_\alpha$ x-ray emission from a Cu foil target irradiated with an ~1-kJ, 10-ps pulse.

compared to a previous design with a 15-μm Au tip.[13] There is a trade-off between having sufficient tip material to delay the breakout and a good electron coupling into the core because more material affects the electron transport and increases the standoff distance from source to core. After imploding the shell with 54 OMEGA UV beams[6] with an energy of ~18 kJ and the drive pulse shown in Fig. 139.34(c), a thin Cu foil was irradiated by the ~1.4-kJ, 10-ps OMEGA EP short-pulse laser.[20] The OMEGA EP laser was defocused to an ~200-μm spot that provided an intensity of ~5×10^{17} W/cm^2 and generated fast electrons with a kinetic energy in the range of several 100 keV to ~MeV (Ref. 21). Strong electrostatic sheath fields at the target boundary retain most of the fast electrons in the ~1-mm foil. The electrons recirculate and generate K$_\alpha$ radiation, providing a relatively uniform Cu K$_\alpha$ area backlighter source. A spherical Bragg crystal imager[22] tuned to the Cu K$_{\alpha1}$ line (8.048 keV) was located on the opposite side of the target and imaged the implosion onto an image-plate detector with a magnification of 14.7. The imaging system efficiently rejects unwanted background and x-ray self-emission from the implosion. The technique also benefits from a higher probing photon energy because the plasma self-emission scales with exp($-h\nu/kT$), where $h\nu$ is the photon energy and kT is the plasma temperature. In shots without a backlighter, the background at 8 keV

caused by self-emission from the implosion was measured to be ~$40\times$ weaker than the signal of the K$_\alpha$ backlighter. Another important parameter for this technique is the emission time of the backlighter, which determines the time resolution because a time-integrating detector was used. Figure 139.34(d) shows a time-resolved measurement of the K$_\alpha$ flash[21] by coupling an ultrafast x-ray streak camera to the Bragg crystal imager. A K$_\alpha$ emission time of 12 ps was quantified, which is short enough to prevent any spatial blurring from the hydrodynamic motion.

First, an image of an undriven target was taken, where the Al tip is clearly visible and less opaque than the gold cone. The image was corrected for spatially varying backlighter intensity, similar to that described in Ref. 16, and for hard x rays that were generated in the foil and scattered in the diagnostic. This shot provided an independent measurement of the magnification of 14.8±0.1 and a measure of the spatial resolution of 22±3 μm. The backlighter was then used to image imploded targets. The time delay between the implosion laser and short-pulse laser was varied on a shot-to-shot basis to probe the fuel assembly at various times [see Figs. 139.35(a)–139.35(e)]. The false color scheme represents the measured optical depth given by $\ln\left(I_0/I\right)$, where I is the measured transmitted signal and I_0 is the measured backlighter intensity. The frame in

E22714JR

Figure 139.35
Flash radiography images of imploded cone-in-shell targets at various stages of the implosion. The probing time was measured *in situ* with ±0.05-ns accuracy at full energy by operating the neutron temporal diagnostic[23] in hard x-ray mode. The top row shows the experimental data at (a) 3.75 ns, (b) 3.82 ns, (c) 3.93 ns, (d) 4.05 ns, and (e) 4.15 ns after the start of the UV drive-laser pulse. The bottom row [(f)–(j)] shows simulated radiographs from 2-D radiation–hydrodynamic simulations. The false color scheme indicates the optical depth.

Fig. 139.35(a) shows the implosion at 3.75 ns after the start of the drive pulse. Time zero is defined as the time when 2% of the peak power from the drive-laser pulse is reached. The fuel starts to assemble in front of the tip and the Al tip was compressed to a higher density, which can be seen when comparing the measured optical depth in the Al tip to that of the undriven target. At later times the Al tip was more deformed and eventually completely destroyed as the fuel assembly reached a higher density. Peak compression was reached at the time of the frame in Fig. 139.35(d) at T_{peak} = 4.05 ns, while the last frame was recorded after peak compression at 4.15 ns. Figures 139.35(f)–139.35(j) display calculated backlighter images for those shots. The simulations were performed with the 2-D radiation–hydrodynamic code *DRACO*[4] in cylindrical geometry and were post-processed with the code *Spect3D*.[24] The simulation capability was significantly improved compared to the results reported in Ref. 13. The radiation transport has been included, the Eulerian scheme improved, and nonlocal thermal electron transport[25] and cross-beam energy transfer[26] accounted for. The simulations compare well with the measured images, revealing similar structure and size of the imploded plastic material. The simulated optical densities agree to better than 10% with the measured optical densities. Slight differences are observed in the shape of the high-density region, which might be caused by three-dimensional (3-D) effects that were not taken into account in the simulations. For late times, some differences are observed in the region between the destroyed Al tip and the dense plasma core. While the simulations show a distinctive gap, the gap is less pronounced in the measurements, which could be a result of turbulent plasma behavior and some mixing of ablated Al material with the plastic. No significant mixing of aluminum and plastic material is noticed in the 2-D simulations but could be stronger in reality. Slight shot-to-shot differences in the deformation of the Al tip do not affect the overall performance of the implosion.

The measured optical-depth distribution was used to infer time-resolved radial density distributions and time-resolved areal densities under the assumption of cylindrical symmetry of the plasma along the cone axis. The optical depth τ is given by the integral over the absorption coefficient κ along the path of an x-ray photon through the dense plasma $\tau = \int \kappa(x)dx$, measured at the specific backlighter photon energy. Vertical lineout profiles $\tau(y)$ (see Fig. 139.36) taken through the dense core show maximum values of up to 1.65±0.1 and a full width at half maximum (FWHM) as small as ~80 μm. Those profiles were Abel inverted to infer κ. The absorption coefficient is equal to the product of the mass-absorption coefficient μ and the mass density ρ, where μ is a function of plasma electron temperature
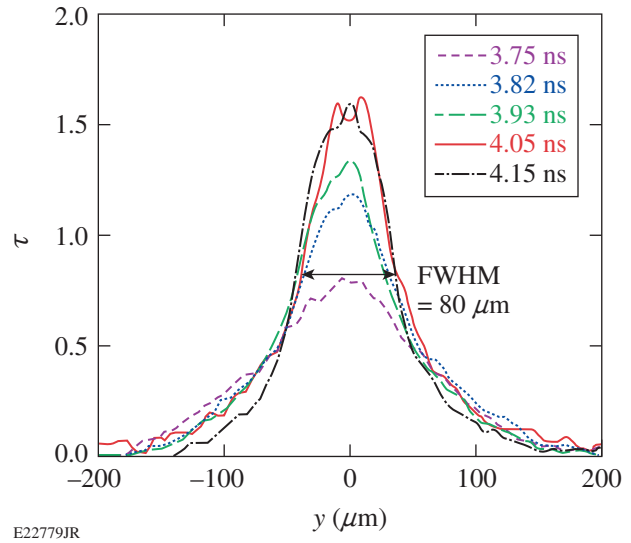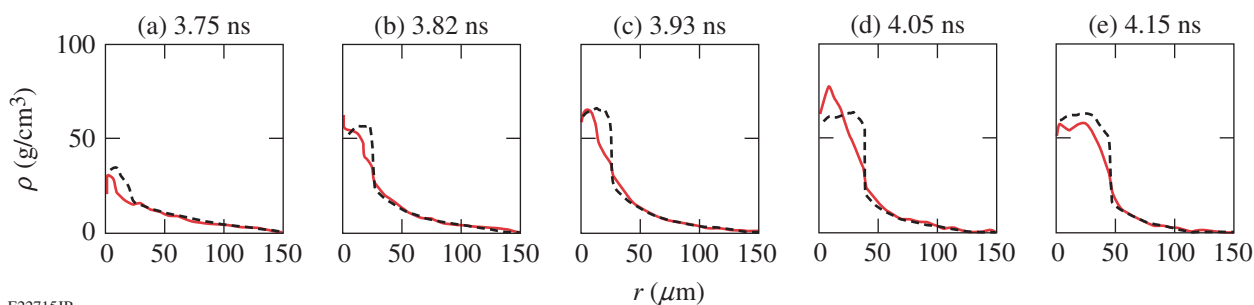

Figure 139.36
Time-resolved optical-depth lineouts through the dense core of compressed plastic measured at a photon energy of 8.048 keV.

T_e and ρ. A steady-state nonlocal thermal electron calculation of μ was performed and the density profile was inferred by dividing κ by μ. Inferred and simulated $\rho(r)$ are compared in Figs. 139.37(a)–139.37(e) at various times. They are very similar for radii larger than 50 μm but show slight differences in the dense region. The inferred $\rho(r)$ is integrated to obtain ρR, which is compared to the predicted value [Fig. 139.38(a)]. The measured areal densities agree with the simulations to better than 15%. A simple expression for maximum ρR was derived in Ref. 27 for an imploded DT capsule filled with 1 atm of DT gas, which makes it possible for the maximum ρR to be scaled with the drive laser energy E_L, the laser wavelength λ, and the adiabat α_{inn} of the inner portion of the shell:

$$(\rho R)_{max}\ (\mathrm{mg/cm}^2) \approx 260\ E_L^{1/3}\ (\mathrm{kJ}) \frac{[0.35/\lambda(\mu\mathrm{m})]^{0.25}}{\alpha_{inn}^{0.54}}.$$

For the current experiment, E_L = 18 kJ and α_{inn} = 3.5, for which the simple expression yields ~350 mg/cm², only ~17% higher than the actual value, showing that the scaling model can be used to estimate the expected $(\rho R)_{max}$ for different energies and adiabats. For a laser energy of 1.9 MJ, which was used in a recent experiment[8] at the National Ignition Facility, and for α_{inn} = 3.5, a value of $(\rho R)_{max} \sim$ 1600 mg/cm² is estimated, which is a factor of ~4.6 higher than with OMEGA. A higher areal density allows for particle stopping up to a higher kinetic energy and, given a certain distribution of kinetic energies, relaxes the requirement to ignite the fuel.

E22715JR

Figure 139.37
Measured (solid) and simulated (dashed) density profiles perpendicular to the cone axis for various times.
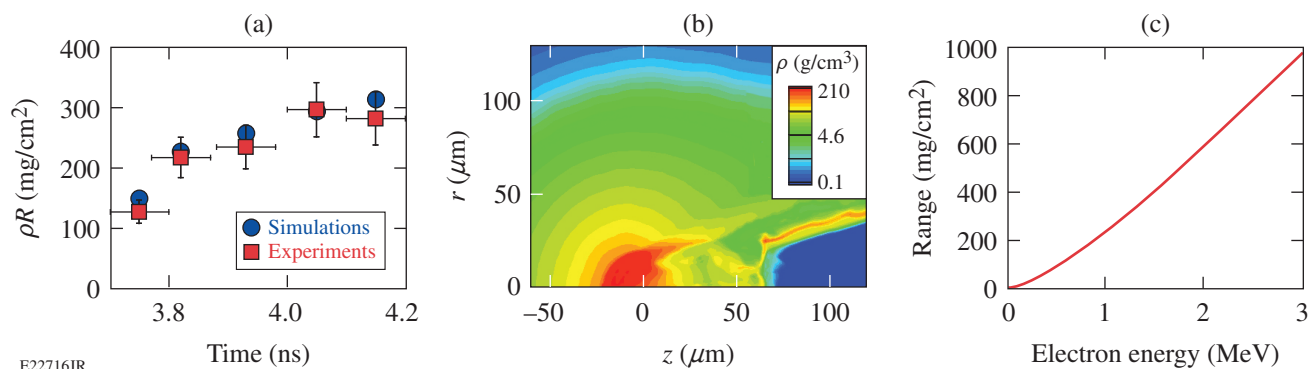
E22716JR

Figure 139.38
(a) Measured (squares) and simulated (circles) areal density perpendicular to the cone axis for various times. (b) Simulated mass-density distribution of the improved implosion at the time of shock breakout at 3.96 ns, which provides an areal density of 500 mg/cm^2. (c) Calculated range of fast electrons in compressed deuterated plastic.

In addition, the breakout time of the shock driven through the cone tip was measured independently, similar to experiments that were described in detail in Refs. 13 and 19. The shots were performed by firing only the OMEGA beams and switching off the OMEGA EP beam. The compressing shell pushed a jet of plasma material toward the cone tip and created a shock wave through the cone wall. When the shock wave reached the inner cone surface, it generated optical emission, which was measured temporally and spatially resolved from the inside with a streaked optical pyrometer[28] and two velocity interferometer systems for any reflector.[29] The measured average breakout time from three implosions was $T_{shock} = 3.85 \pm 0.04$ ns, which agrees well with the predicted value of 3.84 ns. The target is more resilient against the strong shock from the implosion than a previous design with a gold-only cone.[13] Those experiments measured the breakout time for various gold-cone tips with thicknesses from 5 to 15 μm and demonstrated a later breakout for thicker tips. For a 15-μm thickness, the breakout time was 3.76 ns. Therefore, the target

with the 60-μm-thick Al tip improved the margin for the arrival of the short-pulse laser by ~90 ps, bringing the ρR at 3.85 ns to ~200 mg/cm^2 [Fig. 139.38(a)], which is ~70% of the peak ρR.

Our simulations indicate that an even higher ρR might be achievable on OMEGA by removing the air from the shell and reducing the power of the laser pulse picket. Figure 139.38(b) shows the calculated mass-density map at shock breakout for the improved design. The mass and energy of the hot spot are decreased, which delays the cone-tip breakout by reducing the pressure on the cone tip. Fuel stagnation is closer to the target center with a higher density and higher areal density. It brings the shock breakout as close as 80 ps to the peak compression time. At the time of shock breakout, the areal density reaches 500 mg/cm^2, 83% of $\rho R_{max} = 600$ mg/cm^2. It is important to note that such high areal densities provide sufficiently dense plasma to stop fast electrons. Figure 139.38(c) shows the calculated average range of fast electrons in compressed deuterated plastic including blooming and straggling.[30] Electrons up to

1.8 MeV will completely range out in a $\rho R = 500$-mg/cm^2 plastic plasma, while a 200-mg/cm^2 plasma stops electrons up to 0.9 MeV.

In conclusion, a spherical plastic shell with a re-entrant cone was successfully compressed to a high areal density ($\sim$300 mg/cm^2) at a distance of $\sim$50 μm in front of the cone tip, which provides sufficient stopping power for $\sim$MeV electrons—a characteristic that is required for subsequent ignition with a short-pulse ($\sim$ps) laser.

REFERENCES

1. R. P. Drake, *High-Energy-Density Physics: Fundamentals, Inertial Fusion, and Experimental Astrophysics*, Shock Wave and High Pressure Phenomena (Springer, Berlin, 2006).

2. B. A. Remington, R. P. Drake, and D. D. Ryutov, Rev. Mod. Phys. **78**, 755 (2006).

3. J. Nuckolls *et al.*, Nature **239**, 139 (1972).

4. P. B. Radha, T. J. B. Collins, J. A. Delettrez, Y. Elbaz, R. Epstein, V. Yu. Glebov, V. N. Goncharov, R. L. Keck, J. P. Knauer, J. A. Marozas, F. J. Marshall, R. L. McCrory, P. W. McKenty, D. D. Meyerhofer, S. P. Regan, T. C. Sangster, W. Seka, D. Shvarts, S. Skupsky, Y. Srebro, and C. Stoeckl, Phys. Plasmas **12**, 056307 (2005).

5. M. Tabak *et al.*, Phys. Plasmas **1**, 1626 (1994).

6. T. R. Boehly, D. L. Brown, R. S. Craxton, R. L. Keck, J. P. Knauer, J. H. Kelly, T. J. Kessler, S. A. Kumpan, S. J. Loucks, S. A. Letzring, F. J. Marshall, R. L. McCrory, S. F. B. Morse, W. Seka, J. M. Soures, and C. P. Verdon, Opt. Commun. **133**, 495 (1997).

7. E. I. Moses *et al.*, Phys. Plasmas **16**, 041006 (2009).

8. O. A. Hurricane *et al.*, Nature **506**, 343 (2014).

9. R. Betti, C. D. Zhou, K. S. Anderson, L. J. Perkins, W. Theobald, and A. A. Solodov, Phys. Rev. Lett. **98**, 155001 (2007).

10. R. Kodama *et al.*, Nature **412**, 798 (2001).

11. R. Kodama *et al.*, Nature **418**, 933 (2002).

12. S. Atzeni and J. Meyer-ter-Vehn, *The Physics of Inertial Fusion: Beam Plasma Interaction, Hydrodynamics, Hot Dense Matter*, International Series of Monographs on Physics (Clarendon Press, Oxford, 2004).

13. W. Theobald, A. A. Solodov, C. Stoeckl, K. S. Anderson, R. Betti, T. R. Boehly, R. S. Craxton, J. A. Delettrez, C. Dorrer, J. A. Frenje, V. Yu. Glebov, H. Habara, K. A. Tanaka, J. P. Knauer, R. Lauck, F. J. Marshall, K. L. Marshall, D. D. Meyerhofer, P. M. Nilson, P. K. Patel, H. Chen, T. C. Sangster, W. Seka, N. Sinenian, T. Ma, F. N. Beg, E. Giraldez, and R. B. Stephens, Phys. Plasmas **18**, 056305 (2011).

14. Y. Arikawa *et al.*, Bull. Am. Phys. Soc. **58**, 372 (2013).

15. O. L. Landen *et al.*, Rev. Sci. Instrum. **72**, 627 (2001).

16. F. J. Marshall, P. W. McKenty, J. A. Delettrez, R. Epstein, J. P. Knauer, V. A. Smalyuk, J. A. Frenje, C. K. Li, R. D. Petrasso, F. H. Séguin, and R. C. Mancini, Phys. Rev. Lett. **102**, 185004 (2009).

17. R. B. Stephens *et al.*, Phys. Rev. Lett. **91**, 185001 (2003).

18. R. B. Stephens, S. P. Hatchett, M. Tabak, C. Stoeckl, H. Shiraga, S. Fujioka, M. Bonino, A. Nikroo, R. Petrasso, T. C. Sangster, J. Smith, and K. A. Tanaka, Phys. Plasmas **12**, 056312 (2005).

19. C. Stoeckl, T. R. Boehly, J. A. Delettrez, S. P. Hatchett, J. A. Frenje, V. Yu. Glebov, C. K. Li, J. E. Miller, R. D. Petrasso, F. H. Séguin, V. A. Smalyuk, R. B. Stephens, W. Theobald, B. Yaakobi, and T. C. Sangster, Plasma Phys. Control. Fusion **47**, B859 (2005).

20. L. J. Waxer, D. N. Maywar, J. H. Kelly, T. J. Kessler, B. E. Kruschwitz, S. J. Loucks, R. L. McCrory, D. D. Meyerhofer, S. F. B. Morse, C. Stoeckl, and J. D. Zuegel, Opt. Photonics News **16**, 30 (2005).

21. P. M. Nilson, J. R. Davies, W. Theobald, P. A. Jaanimagi, C. Mileham, R. K. Jungquist, C. Stoeckl, I. A. Begishev, A. A. Solodov, J. F. Myatt, J. D. Zuegel, T. C. Sangster, R. Betti, and D. D. Meyerhofer, Phys. Rev. Lett. **108**, 085002 (2012).

22. C. Stoeckl, G. Fiksel, D. Guy, C. Mileham, P. M. Nilson, T. C. Sangster, M. J. Shoup III, and W. Theobald, Rev. Sci. Instrum. **83**, 033107 (2012).

23. R. A. Lerche, D. W. Phillion, and G. L. Tietbohl, Rev. Sci. Instrum. **66**, 933 (1995).

24. J. J. MacFarlane *et al.*, High Energy Density Phys. **3**, 181 (2007).

25. V. N. Goncharov, T. C. Sangster, P. B. Radha, R. Betti, T. R. Boehly, T. J. B. Collins, R. S. Craxton, J. A. Delettrez, R. Epstein, V. Yu.

Glebov, S. X. Hu, I. V. Igumenshchev, J. P. Knauer, S. J. Loucks, J. A. Marozas, F. J. Marshall, R. L. McCrory, P. W. McKenty, D. D. Meyerhofer, S. P. Regan, W. Seka, S. Skupsky, V. A. Smalyuk, J. M. Soures, C. Stoeckl, D. Shvarts, J. A. Frenje, R. D. Petrasso, C. K. Li, F. Séguin, W. Manheimer, and D. G. Colombant, Phys. Plasmas **15**, 056310 (2008).

26. D. H. Froula, I. V. Igumenshchev, D. T. Michel, D. H. Edgell, R. Follett, V. Yu. Glebov, V. N. Goncharov, J. Kwiatkowski, F. J. Marshall, P. B. Radha, W. Seka, C. Sorce, S. Stagnitto, C. Stoeckl, and T. C. Sangster, Phys. Rev. Lett. **108**, 125003 (2012).

27. R. Betti and C. Zhou, Phys. Plasmas **12**, 110702 (2005).

28. J. E. Miller, T. R. Boehly, A. Melchior, D. D. Meyerhofer, P. M. Celliers, J. H. Eggert, D. G. Hicks, C. M. Sorce, J. A. Oertel, and P. M. Emmel, Rev. Sci. Instrum. **78**, 034903 (2007).

29. P. M. Celliers, D. K. Bradley, G. W. Collins, D. G. Hicks, T. R. Boehly, and W. J. Armstrong, Rev. Sci. Instrum. **75**, 4916 (2004).

30. A. A. Solodov and R. Betti, Phys. Plasmas **15**, 042707 (2008).